Ecological Informatics 18 (2013) 69–78

Contents lists available at SciVerse ScienceDirect

Ecological Informatics

journal homepage: www.elsevier.com/locate/ecolinf

Modeling winter wheat phenology and carbon dioxide fluxes at the ecosystem scale based on digital photography and eddy covariance data ☆

Lei Zhou [a,b], Hong-lin He [a,*], Xiao-min Sun [a], Li Zhang [a], Gui-rui Yu [a], Xiao-li Ren [a,b], Jia-yin Wang [a], Feng-hua Zhao [a]

[a] Key Laboratory of Ecosystem Network Observation and Modeling, Institute of Geographic Sciences and Natural Resources Research, Chinese Academy of Sciences, Beijing 100101, China
[b] University of Chinese Academy of Sciences, Beijing 100049, China

ARTICLE INFO

Article history:
Received 24 November 2012
Received in revised form 8 May 2013
Accepted 9 May 2013
Available online 23 May 2013

Keywords:
Digital camera
Greenness index
Phenological date
Gross primary production
Winter wheat

ABSTRACT

Recent studies have shown that the greenness index derived from digital camera imagery has high spatial and temporal resolution. These findings indicate that it can not only provide a reasonable characterization of canopy seasonal variation but also make it possible to optimize ecological models. To examine this possibility, we evaluated the application of digital camera imagery for monitoring winter wheat phenology and modeling gross primary production (GPP).

By combining the data for the green cover fraction and for GPP, we first compared 2 different indices (the ratio greenness index (green-to-red ratio, G/R) and the relative greenness index (green to sum value, G%)) extracted from digital images obtained repeatedly over time and confirmed that G/R was best suited for tracking canopy status. Second, the key phenological stages were estimated using a time series of G/R values. The mean difference between the observed phenological dates and the dates determined from field data was 3.3 days in 2011 and 4 days in 2012, suggesting that digital camera imagery can provide high-quality ground phenological data.

Furthermore, we attempted to use the data (greenness index and meteorological data in 2011) to optimize a light use efficiency (LUE) model and to use the optimal parameters to simulate the daily GPP in 2012. A high correlation ($R^2 = 0.90$) was found between the values of LUE-based GPP and eddy covariance (EC) tower-based GPP, showing that the greenness index and meteorological data can be used to predict the daily GPP. This finding provides a new method for interpolating GPP data and an approach to the estimation of the temporal and spatial distributions of photosynthetic productivity.

In this study, we expanded the potential use of the greenness index derived from digital camera imagery by combining it with the LUE model in an analysis of well-managed cropland. The successful application of digital camera imagery will improve our knowledge of ecosystem processes at the temporal and spatial levels.

1. Introduction

Phenology is the study of the timing of recurring biological events and the causes of the changes in this timing produced by biotic and abiotic factors (Lieth, 1976; Zhu and Wan, 1973). Phenological studies have a long tradition in agriculture. The knowledge of the annual timing of crop phenological stages and their variability can help to improve crop yield and food quality by providing dates for timely irrigation, fertilization, and crop protection (Mirjana and Vulić, 2005). In agro-meteorological studies, phenological data are used to analyze crop–weather relationships and to describe or model the phyto-climate (Frank, 2003). Furthermore, phenological data are one of the most important components of ecosystem and dynamic vegetation models (Arora and Boer, 2005; Dragoni et al., 2011). Only accurate descriptions of phenology and canopy development in ecosystem models can produce reasonable carbon budgets at regional and global scales (Gitelson et al., 2012; Richardson et al., 2012). Thus, the ability to accurately model and predict seasonal canopy development is essential.

Generally, 2 methods are used to acquire phenological data: direct observation and satellite-based observation. Phenological field stations that rely on data gathered by direct human observation provide relatively accurate phenological stages (Bowers and Dimmitt, 1994;

Abbreviations: GPP, gross primary production; LUE, light use efficiency; AVHRR, advanced very high-resolution radiometer; MODIS, moderate resolution imaging spectroradiometer; NEE, net ecosystem exchange; APAR, amount of photosynthetic radiation absorbed; VPM, vegetation photosynthesis model; DOY, day of year; ROI, region of interest.

* Corresponding author. Tel.: +86 10 6488 9599; fax: +86 10 6488 9399.
E-mail address: hehl@igsnrr.ac.cn (H. He).

1574-9541/$ – see front matter © 2013 . Published by Elsevier B.V. All rights reserved.
http://dx.doi.org/10.1016/j.ecoinf.2013.05.003

Menzel and Fabian, 1999). However, the sparsely distributed stations located in limited geographical areas have poor spatial coverage, and phenological data are inadequate to characterize the continuous development of vegetation (Schwartz et al., 2002; White et al., 2005). Although remote sensing data from sources such as the advanced very high-resolution radiometer (AVHRR), the moderate resolution imaging spectroradiometer (MODIS), and Landsat are used in detecting spatial patterns of global-scale phenology (Ganguly et al., 2010; Heumann et al., 2007; Moulin et al., 1997; Soudani et al., 2012; Zhu et al., 2012), exogenous factors such as atmospheric effects (e.g., cloud contamination, haze) and data processing methods limit the quality of satellite observations and produce variation in the results. For this reason, there remains a crucial need for precise field data that can be used to understand and validate satellite data (Studer et al., 2007). In this context, the most important point is the large gap between spatially integrated information from satellite sensors and point observations of phenological events at the species level (Linderholm, 2006; Schwartz and Reed, 1999).

In the past few years, significant improvements in electronic imaging technologies have made digital camera technology increasingly popular. As a new method for near-surface remote sensing, digital camera technology, which combines the advantages of traditional field phenological observations with remote sensing observations, has shown great potential in monitoring phenological events in various ecosystems including forests and grassland (Fisher et al., 2006; Hufkens et al., 2012; Richardson et al., 2009; Saitoh et al., 2012; Wingate et al., 2008).

Recently, the relationship between the timing of phenological events and carbon flux has received increasing attention (Ahrends et al., 2009; Baldocchi et al., 2001; Kindermann et al., 1996). Previous research has indicated that farmland ecosystems, especially in mid-latitudes, contribute substantially to the regional carbon dioxide budget (Soegaard et al., 2003). As a key parameter of the carbon cycle, GPP can be used to evaluate the effects of climate variation or crop management on food production. However, the lack of an accurate description of phenology and canopy status in ecosystem models restricts the accuracy of GPP simulations. Thus, to develop improved simulation models of carbon flux, we need more accurate seasonal phenological data for the canopy (Chiang and Brown, 2007). Real-time canopy status information extracted from digital camera photography can allow the optimization of GPP models. To the best of our knowledge, data derived from digital camera images have seldom been used in efforts to optimize GPP models (Migliavacca et al., 2011). As a common method of estimating GPP, the light use efficiency (LUE) model has been used at various scales. Optimizing the LUE model based on canopy greenness data obtained from digital photography and on CO_2 flux measured from eddy covariance towers might be useful for several reasons. First, this approach might augment the methodology used to acquire data for ecological studies. Second, it might improve the accuracy of modeling canopy phenology and daily GPP at the ecosystem scale.

In China, phenological stations and conventional phenological data are relatively scarce. Both are associated primarily with natural ecosystems; in contrast, they seldom offer phenological coverage of farmland (Chen et al., 2005). The North China Plain is situated on sediments deposited by the Yellow River and is located between 114–121°E and 32–40°N. It includes 2 metropolitan centers (Beijing and Tianjin) and 5 provinces (Anhui, Hebei, Henan, Jiangsu, and Shandong; Liu et al., 2001). It is the largest and most important agricultural area of China and is also known as the "Granary of China." It encompasses an agricultural area of approximately 1.8×105 km^2 (Wu et al., 2006), producing more than 50% of the nation's wheat supply (Kendy et al., 2003). To date, to the best of our knowledge, no attempts have been made to use digital camera imagery to monitor crop phenology and optimize carbon dioxide flux models in China.

In this study, we analyzed time series of color indices of winter wheat obtained from digital camera imagery during 2011 and 2012. Our primary goal is to address the following research questions: (1) Can digital camera imagery be used to characterize the seasonal dynamics of winter wheat? (2) Can digital camera imagery be used as an additional source to evaluate the potential of the LUE model for estimating the daily GPP of winter wheat at the site level? The aim of the study is to create a Digital Camera Phenological Observation Network in China and to increase the understanding of the seasonal covariation between GPP and phenology at the ecosystem scale.

2. Materials and methods

2.1. Site description

The study was conducted at Yucheng Comprehensive Experimental Station (36°27′N, 116°38′E, 20 m elevation), located in the North China Plain within the East Asian Monsoon region. The climate of this region is warm temperate and semi-humid. Over the past 30 years, the mean temperature and mean precipitation of this area were approximately 13.1 °C and 528 mm, respectively. Nearly 60% of the summer precipitation occurs from June through August. The parent soil materials are alluviums from the Yellow River. The soil texture of the root zone is sandy loam (Li et al., 2006). Winter wheat (*Triticum aestivum L*) is usually sown in early October and harvested in mid-June. The life cycle of winter wheat is shown in Table 1.

2.2. Camera images and image analysis

Canopy images were collected using a commercial webcam (model 214; Axis Communications, Lund, Sweden) installed in a weatherproof enclosure at a height of 4 m above the ground. The camera featured a Sony Corp. 1/4″ Wfine progressive scan red-green-blue (RGB) silicon charge-coupled device. The red, green, and blue channels had peak sensitivities at wavelengths of 620, 540, and 470 nm, respectively (full technical specifications are available online, http://www.sony.net/Products/SC-HP/datasheet/90203/data/a6811217.pdf).

The camera provided half-hourly JPEG images (image resolution of 384 * 288 with 3 color channels of 8-bit RGB color information, i.e., digital numbers ranging from 0 to 255) from 8:30 to 17:00 h local time every day. The image covered an area of approximately 30 m^2. The raw images were transmitted via wireless networks and automatically stored in a personal computer. The filenames included a date and time stamp for subsequent processing.

In this study, we collected 2238 images in 2011 and 1981 images in 2012. On average, 17 images were collected per day; however, unavoidable network connectivity problems resulted in occasional gaps in the webcam data recordings. The data for 19 days (12%) and 21 days (13%) were missing in 2011 and 2012, respectively. The longest gap without a picture was 7 days in 2011 and 15 days in 2012.

The image quality was occasionally adversely affected by variable light conditions or by condensation on the window housing the camera. However, no selective editing or artificial enhancement of any of the archived images was performed before the image analysis. This procedure allowed us to compare the results with those obtained from different sites or reported by other studies.

The image data were processed using a program written in Matlab (R2009a; The Math Works, Natick, Mass., USA). The camera images were successively loaded, and the date and time were extracted from the filename. First, a subset of each image was selected as a region of interest (ROI) because each population is known to show spatial heterogeneity. The winter wheat showed homogeneous growth within the coverage represented by a single photo. Accordingly, the entire image was selected as an ROI. Second, color channel information (digital numbers: DNs) was extracted from the images and averaged across the ROIs for each of the 3 color channels (red DNs, green DNs, and blue DNs). Furthermore, the camera-based greenness indices

Table 1
The life cycle of winter wheat.

Crop	The life cycle								
Winter wheat	Seeding time	Time of emergence	Trefoil stage	Tillering stage	Green returned stage	Jointing stage	Heading stage	Dough stage	Harvest time

(G%, G/R) for each photograph were calculated using the following equations (Adamsen et al., 1999; Ahrends et al., 2008):

$$G\% = \frac{\text{Green DN}}{\text{Red DN} + \text{Greeen DN} + \text{Blue DN}} \quad (1)$$

$$G/R = \text{Green DN}/\text{Red DN}, \quad (2)$$

where G% and G/R are the greenness indices for the ROI of each photograph and Red DN, Green DN, and Blue DN are the DN values of the blue, green, and red channels.

2.3. Eddy covariance flux measurement and micrometeorological data

An eddy covariance (EC) system and a microclimate gradient measurement system were placed in the center of a large crop field. The EC system consists of a 3-dimensional sonic anemometer and an open-path infrared CO_2/H_2O analyzer (IRGA. Li-7500; Li-Cor Inc., Lincoln, Nebraska, USA) at a height of 2.80 m; this system measures the fluctuations in wind velocity, temperature, water vapor, and CO_2 concentration. All the data were collected continuously at 10 Hz with a Campbell Scientific data logger (model CR5000; Campbell Sci. Inc., Utah, USA), and the 30-min mean data were output (Qin et al., 2005).

The microclimate gradient measurement system includes anemometers (model AR-100; Vector Instruments, UK) and psychrometers (model HPM-45C; Vaisala, Finland) placed at average heights of 2.20 and 3.40 m, respectively. Photosynthetically active radiation was measured using a quantum sensor (Li-190SB; Li-Cor Inc., USA). For a complete description of the arrangement of these instruments, see Li et al. (2006).

2.4. Thresholds for detecting key phenological stages

Key phenological stages are periods in which canopy greenness changes markedly and farmland management has a significant effect on farm crop yield. In this study, the key phenological stages for winter wheat were the greenup stage, the jointing stage, and the harvest time. (1) During the greenup stage, winter wheat begins to green up from winter dormancy, and green leaves rapidly appear. Therefore, the smoothed time profile of the greenness index was assumed to increase rapidly during this stage. The date of the most rapid increase in the greenness index in the time profile was used as the estimate of the onset of the greenup stage. (2) The jointing stage is the stage at which the internodal tissue in the winter wheat leaf begins to elongate and forms a stem. In this phase, the growth phase of the winter wheat changes from vegetative to reproductive. This stage represents a plateau with a high value of the greenness index. Therefore, we defined the date on which the curvature of the greenness index reaches its second maximum as the estimated onset of the jointing stage. (3) The harvest time is the date on which the wheat is reaped. The greenness index gradually decreases as the leaves wither and die. An abrupt decrease in the greenness index follows due to harvesting. Therefore, the date corresponding to the inflection point at which the curvature reaches its last maximum was defined as the estimated harvesting date.

First, the double logistic function was used to fit the time series of the greenness index because this function can express the growth process continuously, as shown in Eq. (3). The curvature (ρ) of the fitted time series for the greenness index was then calculated (Eq. (4)) as follows:

$$g(t) = a + \frac{b}{[1 + \exp(c - dt)][1 + \exp(e - ft)]} \quad (3)$$

$$\rho = \left| \frac{g(t)''}{\left(1 + g(t)'^2\right)^{\frac{3}{2}}} \right|, \quad (4)$$

where $g(t)$ is the fitted greenness index, t is the driving variable (day of year, DOY), and a through f are parameters of the fitted function. Parameters a and b are the base levels (e.g., the dormant season value) of $g(t)$ and the seasonal amplitude of $g(t)$, respectively. Parameters c and d control the phase and slope for the greenup stage, and parameters e and f control the timing and rate of decrease associated with senescence. $g(t)' = dg(t)/d(t)$ denotes the first derivative of $g(t)$ with respect to t; $g(t)'' = d^2g(t)/d(t)^2$ denotes the second derivative of $g(t)$ with respect to t.

2.5. LUE model

The LUE model was proposed by Monteith (Monteith, 1972) and has been extensively used to estimate GPP at various temporal and spatial scales (Sims et al., 2005; Turner et al., 2003). This model assumes that carbon fixation is linearly related to LUE and to the amount of photosynthetic radiation absorbed (APAR), which is the product of photosynthetically active radiation (PAR) and the fraction of PAR absorbed (FPAR; Heinsch et al., 2003). The APAR in the LUE model can be estimated from daily meteorology (Veroustraete et al., 2002) or can be obtained through the use of a vegetation index related to photosynthetic efficiency (Gamon et al., 1997). In this study, GI (Greenness Index) was used as a proxy of FPAR.

$$GPP_i = \varepsilon_{max} \times (\alpha + \beta \times GI_i) \times PAR \times f(VPD) \times f(T_{min}), \quad (5)$$

where ε_{max} is the maximum light use efficiency ($gCMJ^{-1}$), with an assumed value of 3.47 $gCMJ^{-1}$ (Yan et al., 2009); $f(T_{min})$ and $f(VPD)$ are linear threshold functions that range between 0 and 1 and that express the effects of suboptimal temperatures and water availability for photosynthesis, respectively; PAR is the incident PAR (MJm^{-2}); and parameters α and β were estimated from the observed daily GPP.

The function $f(T_{min})$ used to describe the influence of T_{min} is defined as follows:

$$f(T_{min}) = \begin{cases} 0 & \text{if } T_{min} \le T_{mmin} \\ \dfrac{T_{min} - T_{mmin}}{T_{mmax} - T_{min}} & \text{if } T_{mmax} > T_{min} > T_{mmin} \\ 1 & \text{if } T_{min} \ge T_{mmax} \end{cases} \quad (6)$$

where T_{min} is the observed daily minimum temperature and T_{mmax} and T_{mmin} indicate the thresholds between which the constraint varies linearly.

The daily indicator function f(VPD) for water availability has a value of 1 if the daily VPD is lower than the minimum threshold (VPD_{min}) and a value of 0 if the daily VPD is greater than the maximum threshold (VPD_{max}), above which VPD forces stomatal closure. In this study, the values of T_{mmin}, T_{mmax}, VPD_{min}, and VPD_{max} were set according to the MODIS GPP algorithm (Heinsch et al., 2003).

The best-fit model parameters were estimated in Matlab using the Levenberg–Marquardt method. The overall accuracy of the fitted models was evaluated in terms of the fitting statistics (R^2, RMSE) calculated for the observed and modeled data (Janssen and Heuberger, 1995).

3. Results

3.1. Qualitative patterns

A substantial number of images were collected during the 2011 and 2012 winter wheat growing seasons. Distinct changes in the wheat canopy can be observed by comparing the images obtained at different times. For example, the seasonal change during the growing season in 2011 is shown in Fig. 1. During the winter and early spring, no green leaves emerged, and the images primarily showed the color of the soil. Thus, it could be inferred that the winter wheat was in a dormant stage. The onset of the greenup stage was marked by a change in image coloration. Although yellow was the principal color, green bands began to appear as the leaves emerged; this pattern was clearly visible by day 66 (Fig. 1A). This finding suggested that the winter wheat was in the greenup stage. The images obtained on day 105 (Fig. 1B) showed that the green color had replaced the yellow color. The green coloration continued to increase with the development of the canopy and reached a peak on day 130 (Fig. 1C). Yellow then became increasingly evident and became the principal color on day 163 (Fig. 1D).

3.2. Quantitative patterns

The following analysis yielded a quantitative description of the canopy. First, the daily greenness indices were calculated using the functions specified by Eqs. (1) and (2). The color channels (R, G, B), brightness index, and greenness index showed substantial diurnal variation, and these patterns of diurnal variation were nearly symmetrical (Fig. 2). The daily minimum values for the greenness indices between 10:00 and 15:00 h local time were adopted as the daily greenness index because the minimum value was observed close to noon, when the solar elevation angle is a minimum. The time series for the color channels (R, G, B) did not show any obvious seasonal trends (Fig. 3A,B), suggesting that the greenness value alone fails to capture the development of the canopy.

The canopy status can be accurately described through the use of the greenness index that can best predict canopy development. The correlations between the ancillary data and the greenness indices are shown in Table 2. There was a positive correlation between cover estimation and GPP. The correlation of G/R with the ancillary data was slightly stronger than that of G%. Therefore, the results are further discussed only in terms of G/R.

In 2011, G/R (Fig. 3C) began increasing gradually after DOY 60 in conjunction with an increase in temperature and reached its maximum at approximately DOY 110. Over the following weeks (at or near DOY 150), G/R showed a marked decline due to the maturation of the winter wheat. This seasonal variation is in accordance with the development of winter wheat. However, a slight decline in G/R was observed before DOY 60 in 2011 (Fig. 3C). This result indicates that the increase in soil moisture caused G/R to decrease. Most likely, this decrease resulted from the increase in soil moisture because the reflectance of G decreased more markedly than that of R, resulting in decreasing brightness values. In 2012, G/R (Fig. 3D) began to increase gradually after DOY 70 with increasing temperatures and then showed the same trend as in 2011, i.e., reached its minimum value on approximately DOY 160.

The G/R time series for the growing season (1 March to 19 June) was fitted using the curve shown in Eq. (3) ($R^2 = 0.90$), and the maximum linear curvature was calculated as shown in Eq. (4). Based on this analysis, the onset dates of the 3 key phenological stages were DOY 66, 105, and 160. The same method was used to obtain the key phenological stages in 2012, as shown in Table 3. The interannual variance of the stages in which greenness reappeared was found to be large. The date at which greenness returned was affected by the temperature, soil moisture, radiation, and sowing dates. The mean difference between the greenness-based phenological dates and the field data was 3.3 days in 2011 and 4 days in 2012. These results further confirmed that the G/R index can be used to obtain relatively accurate phenological stages during winter wheat development.

3.3. Performance of the LUE model

Three LUE models based on different variables were used to model the daily variation in GPP for 2011. The 3 models differed in terms of the impact of different environmental factors on FPAR. Model 1

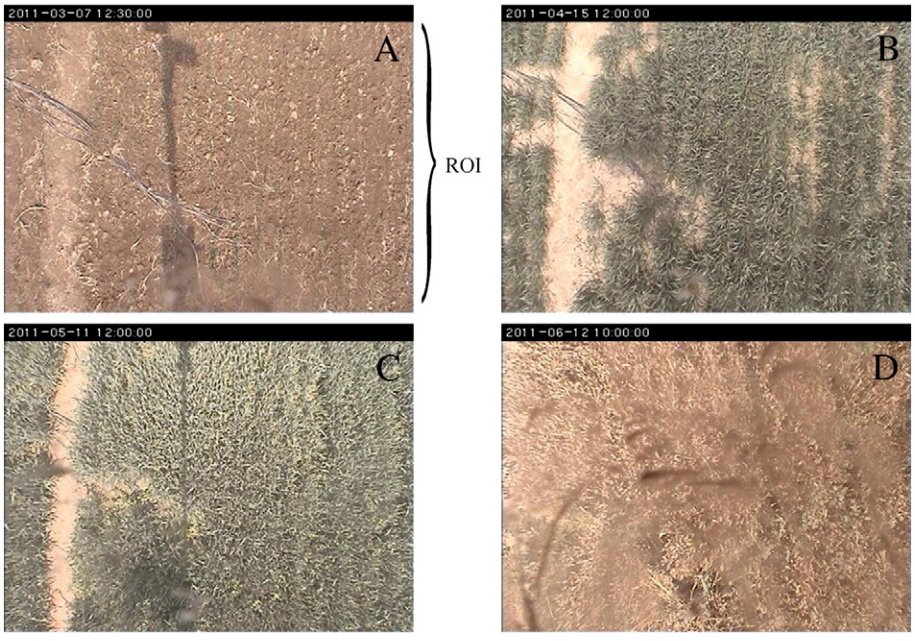

Fig. 1. Sample webcam images of winter wheat. (A) day 66, (B) day 105, (C) day 130, (D) day 163 in 2011. ROI is the region of interest.

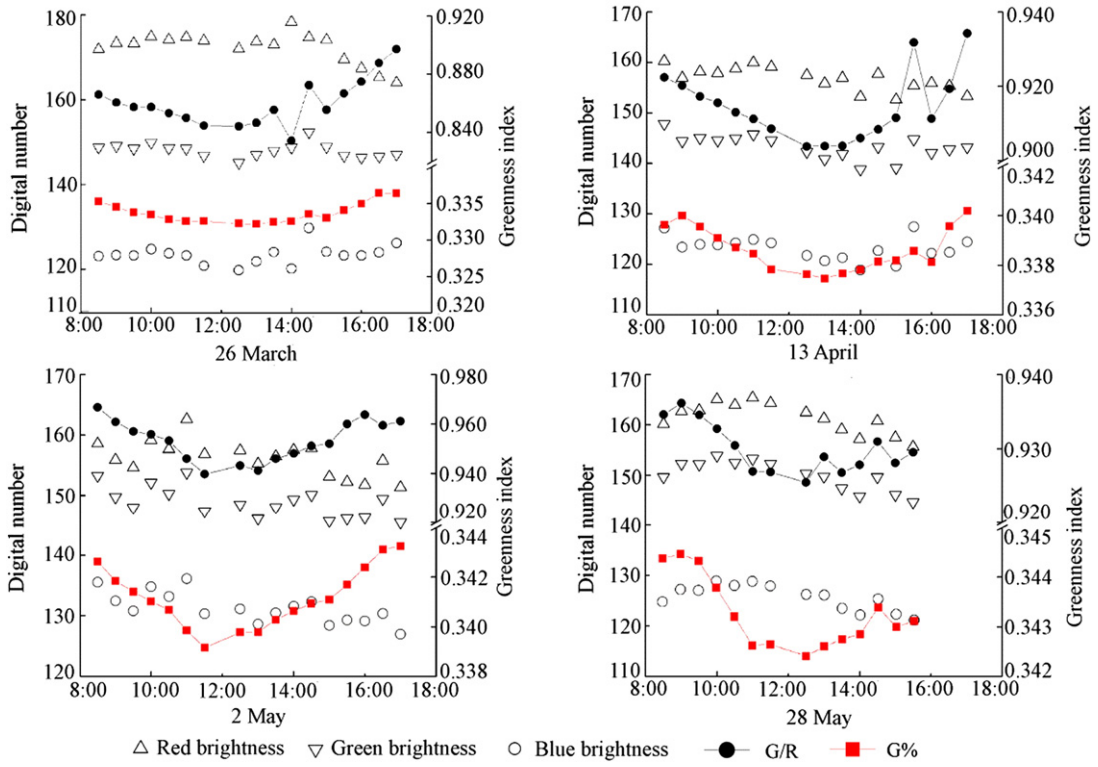

Fig. 2. Diurnal pattern of RGB brightness levels. G/R and G% for winter wheat at different times of the year.

assumed that temperature and VPD jointly affected FPAR, model 2 assumed that only temperature affected FPAR, and model 3 did not include the limited effects of environmental factors on FPAR. To identify the best model, we computed the parameters for the 3 LUE models based on the 2011 data. To compare the 3 GPP models (GPP_{mod}) with the GPP measurements (GPP_{obs}) for 2011, we then computed the correlation coefficients between the model values and the measured values, as well as the associated RMSE (Table 4). The strong correlations found between the GPP_{mod} values and GPP_{obs} showed that color indices (i.e., GI) can be used effectively in combination with meteorological data to describe GPP (Table 4). The comparison of these correlations (Table 4) shows that model 1 is clearly superior to the other 2 models, particularly in view of the strong agreement between model 1 and the measurements (Fig. 4).

To verify the feasibility of different LUE models, we modeled the GPP for the growing season in 2012 based on site-specific data (temperature, VPD, PAR, and greenness indices). The values of parameters α and β for all 3 models are shown in Table 4. The seasonal dynamics of the GPP (GPP_{mod}) predicted by the LUE model was consistent with the observed GPP (GPP_{obs}) values, as shown in a Taylor diagram (Fig. 5). In this diagram, the effectiveness of the 3 models considered in this study is represented by the distance between point A and points B, C, and D. A shorter distance between points indicates a more accurate model. For the 2012 growing season, the diagram clearly shows that point B (model 1) is closest to point A. A simple linear regression model also showed good agreement between point A (GPP_{obs}) and point B (GPP obtained from model 1) for the 2012 growing season (Fig. 6, upper right panel). Furthermore,

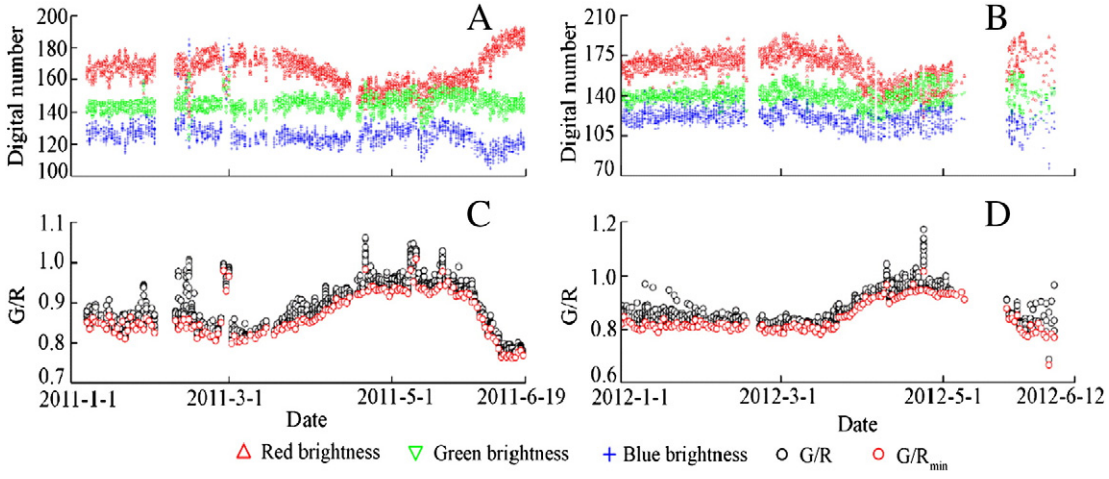

Fig. 3. Time series of brightness numbers (A, B), ratio greenness index (C, D). x axis is day of year.

Table 2
Linear correlation coefficient calculated between ancillary data and greenness indices. GPP was daily averaged from 1 March to 31 May in2011.

	Cover estimation	GPP
G/R	0.957[a]	0.76[a]
G%	0.891[a]	0.74[a]

Cover estimation is percentage of green leaf area in picture, calculated by the software "SAMPLEPOINT" (Booth et al., 2006).
[a] Represents significant correlation ($P < 0.001$).

Table 4
Summary of statistics for identifying the best fit (determination coefficient; r^2, root mean square error, RMSE) of different models, the formula of model 1 is equal to Eq. (5); the formula of model 2 is equal to Eq. (5) remove f(VPD); and the formula of model 3 is equal to Eq. (5) remove f(VPD) and f(T).

	VPD	T	PAR	GI	R^2	RMSE	α	β
model 1	√	√	√	√	0.86	2.5	−0.05748	0.077457
model 2		√	√	√	0.85	2.7	−0.05770	0.075963
model 3			√	√	0.77	3.2	−0.04255	0.054904

point C (model 2) is also close to point B. These comparisons confirm that model 1 is the most reasonable of the 3 models evaluated.

The GPP_{obs} data tended to show an initial increase with a subsequent decrease; the same trend was evident in the GPP_{mod} data (Fig. 6). Furthermore, we calculated the site-scale GPP using the Vegetation Photosynthesis Model (VPM), which has been used at the Yucheng site (a detailed description of the VPM model and its parameters is given in Yan et al., 2009). The results of this calculation showed that the GPP values calculated from LUE model 1 and from the VPM model differed significantly, especially considering the resolution of the data (Fig. 6). The GPP values calculated from the LUE model were represented on a daily scale, whereas the GPP values calculated from the VPM model were represented on an 8-day scale; hence, only 14 values were available from the VPM model for the period from 1 March through 10 June. A statistical analysis showed that the GPP values derived from the LUE model were closer to the GPP_{obs} values than those derived from the VPM model (Table 5, Fig. 6).

4. Discussion

4.1. Effectiveness of digital camera tracking of canopy phenology

Our results suggested that digital camera imagery was well suited for monitoring the development and phenological stages of winter wheat, as reported by many previous studies (Adamsen et al., 1999; Jensen et al., 2007; Lukina et al., 1999). The indices (G/R) derived from the imagery analysis provided reliable information on the daily canopy state. Additionally, they facilitated the continuous and unattended monitoring of the timing and rate of canopy development (Migliavacca et al., 2011), demonstrating the importance of digital camera imagery for canopy tracking.

In general, determining the phenological stages of a canopy using "near-surface" remote sensing is difficult because of the high heterogeneity of the canopy. However, the phenological stages obtained using a digital camera in this study were similar to those observed directly (Table 3); this similarity in the results can be explained in 2 ways. First, the study area was located on the alluvial plain of the Yellow River. The terrain of this area is flat, and hydrothermal conditions are consistent throughout the area, resulting in a relatively uniform agro-ecosystem canopy. Second, the digital camera used in this study provided appropriate technical support. The 3 bands of the digital camera (the red, green, and blue channels) had peak sensitivities at wavelengths of 620, 540, and 470 nm, which corresponded to the absorptive/reflective/absorptive bands of the vegetation. The relative values of reflectance at these wavelengths are normally $R_{540} > R_{620}$ and $R_{540} > R_{470}$ (Serrano et al., 2000). Soil-forming minerals, water content, organic matter, and texture are known to affect the spectral features of soil in a highly complex manner. The relative values of reflectance found by our study were $R_{620} > R_{540} > R_{470}$ on the soil surface (Stoner and Baumgardner, 1981). Hence, the G/R was calculated on the basis of this difference, which describes the absorptive/reflective characteristics of the different bands between the vegetation canopy and the soil surface. Apparently, the gap between the vegetation and the soil was emphasized by the transformation of the banding pattern, providing an effective source of vegetation information.

The use of a digital camera to monitor vegetation phenology has as its primary focus the real-time monitoring of canopy development, namely, the phenological phase (Mirjana and Vulić, 2005), including the various stages of canopy development, such as the jointing stage. G/R was found to be an effective index to track the trajectory of the growing season, as previously reported (Adamsen et al., 1999). The seasonal variations in G/R were, most likely, caused by 2 types of phenological parameters, namely, the leaf area and the physiological pigments (Saitoh et al., 2012). During the growth of winter wheat, the leaf area increases rapidly after winter recovery, reaches a maximum at or near the heading stage (at approximately the end of April in the study area), and then declines gradually as the lower leaves begin to die (Chen et al., 2010). The content of physiological pigments is known to change regularly. These seasonal variations (leaf area and physiological pigments) translate into clear dynamic changes in photosynthetic capacity (Muraoka and Koizumi, 2005). For this reason, the daily NEE and PAR data were collected using the eddy covariance technique, and the Michaelis–Menten equation was used (Hollinger et al., 2004) to obtain a curve for the theoretical light-saturated rate of canopy photosynthesis (A_{max}). A positive relationship was found between G/R and A_{max} (Fig. 7), suggesting that G/R could reflect the phenological activity of the plants at the physiological level.

Table 3
Phenological dates (day of year) derived from digital camera images (Cam) and dates from field observations (Obs).

	Greenup stage (DOY)			Jointing stage (DOY)			Harvest time (DOY)		
	Cam	Obs	Diff	Cam	Obs	Diff	Cam	Obs	Diff
2011	66	62	4	105	102	3	160	163	3
2012	80	73[a]	7	104	99	5	159	159	0

[a] the date was missed and determined by first day of 5-day consecutive mean temperature beyond 3 °C.

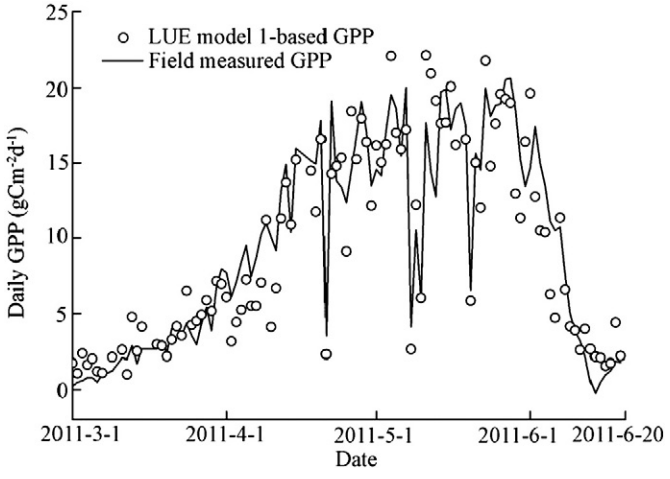

Fig. 4. Seasonal variation in daily GPP values calculated using model 1 and field measured. The hollow circle indicates the modeled values, and the line indicates the field measured values.

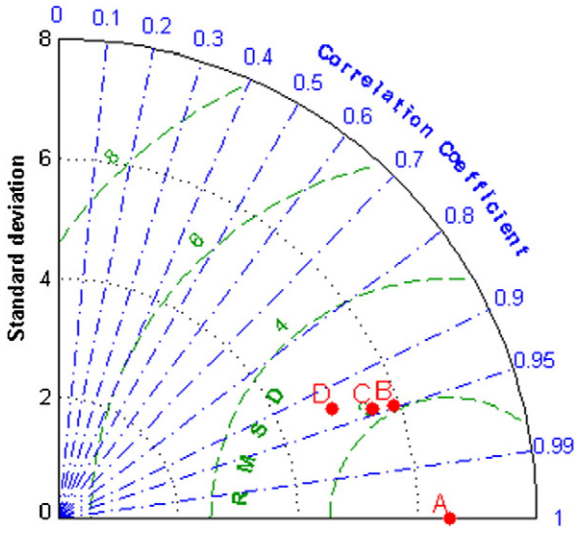

Fig. 5. Pattern statics between field-measured GPP and GPP measured using different models. Letter A stands for filed-observed GPP; letters B, C, and D indicate modeled GPP derived from models 1, 2, and 3, respectively.

4.2. The usefulness of greenness indices for improving GPP modeling

The daily GPP could be estimated with the LUE model based on a combination of the greenness indices and the meteorological data (Table 4, Fig. 6). In 2011, the modeled GPP values were very similar to the observed GPP values resulting from the incorporation of different numbers of constraint factors, as shown by the comparison among the 3 types of LUE models (Table 4). Because model 3 was derived only on the basis of radiation and G/R, the results derived from this model were closer to the potential photosynthetic activity than were those derived using the other models, and the relationship (R^2) with the observed GPP was relatively weak. If a temperature constraint was included (model 2), the relationship (R^2) with the observed GPP improved substantially. However, the inclusion of the VPD constraint (model 1) improved the relationship (R^2) with the observed GPP only slightly. This result indicated that temperature had a profound influence

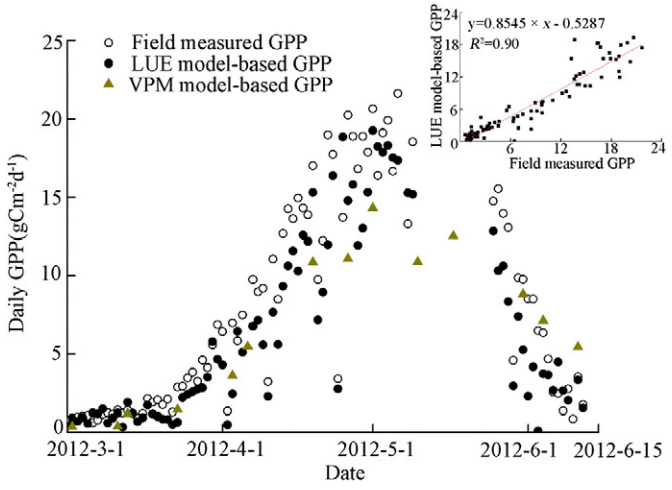

Fig. 6. The comparison between filed-observed GPP and modeled GPP in 2012. The upper right corner is the fitted line between LUE model-based GPP and observed GPP. The data between 10 May and 24 May could not be collected for the LUE model. Hollow circles indicate field-observed daily GPP values, and solid circles indicate LUE model-based GPP values (model 1), upper triangles indicate VPM model-based GPP value. The VPM model was run using site-specific data on temperature, PAR, and vegetation indices in 2012.

Table 5
Summary of statistical variables for GPP_{obs} and GPP_{mod} on the basis of 13 sample data (except the data on 17 May because the LUE model does not include results for this date).

Statistical variables	Obs GPP	LUE model	VPM model
Mean	9.05	6.98	6.23
Standard error	2.12	1.85	1.30
Standard deviation	7.66	6.67	4.70
Minimum	0.90	0.64	0.36
Maximum	20.66	19.27	14.31

on the daily GPP (Table 4). Generally, the principal environmental factors for plant species are temperature, day length, and water availability (Soudani et al., 2012). The content (including the naturally occurring nutrient content) of the soil does not represent an important constraint for plants grown under human management (e.g., due to the use of irrigation and/or fertilizer). Therefore, temperature is an important environmental factor at this well-managed cropland site; it is the only important environmental factor that controls daily GPP (Chen and Xu, 2012; Chmielewski and Rotzer, 2002).

For 2012, a high correlation was found between the measured data and the simulated data from the 3 models, indicating that the parameters derived from the 2011 data were highly suitable for describing the GPP variation in 2012 (Fig. 5). Although all 3 models showed high correlations, model 1 yielded a more accurate determination of the GPP values for winter wheat in 2012. The simulation results obtained with this model are highly accurate and are superior to those obtained from a simulation using the VPM model and 8-day MODIS data (Yan et al., 2009). The VPM model is based on remote sensing data and was developed to estimate the GPP of terrestrial ecosystems (Xiao et al., 2004); this model has been successfully used to estimate GPP in various ecosystems, including forest, grassland (Li et al., 2007), and managed cropland (Yan et al., 2009). In this study, the GPP values based on the LUE model agreed more closely at the ecosystem scale with the observed values than did the GPP values based on the VPM model. The principal reason for this difference could be that the greenness indices derived from digital imagery not only have higher spatial and temporal resolution and are less affected by environmental conditions than MODIS data (Richardson et al., 2007; Studer et al., 2007) but also reflect the photosynthetic capacity of the canopy (Graham et al., 2006; Liu and Pattey, 2010; Pekin and Macfarlane, 2009). Additionally, the effects of a water deficit were represented by VPD in the LUE model, whereas they were represented by the land surface water index (LSWI) derived from MODIS reflectance in the VPM model. Although the LSWI is sensitive to the total amount of liquid water in the crop (Chandrasekar et al., 2010), it is easily affected by exogenous factors.

The greenness indices were found to be extremely valuable for developing and testing the LUE model for monitoring daily GPP. This approach might be useful for developing a new method to interpolate the GPP data regardless of data loss and might furnish a method for estimating the temporal and spatial distributions of photosynthetic productivity (Saitoh et al., 2012).

4.3. Uncertainty and limitations

Previous studies have suggested the use of digital imagery for monitoring seasonal variations in the structure of the plant canopy (Crimmins and Crimmins, 2008; Kawashima and Nakatani, 1998; Liu and Pattey, 2010; Richardson et al., 2007; Sakamoto et al., 2011). In this study, we highlighted the potential use of digital imagery for the development and parameterization of LUE models for winter wheat. Nevertheless, this method, incorporating RGB color imagery data to obtain vegetation status, is not perfect due to several limitations and uncertainties. These limitations need to be addressed to

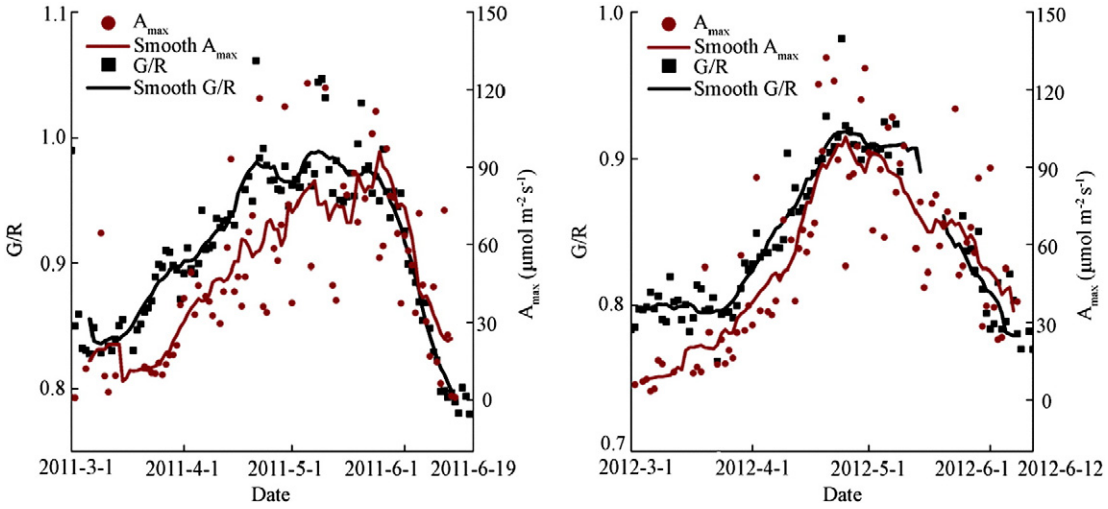

Fig. 7. Seasonal variation of greenness indices (G/R) and A_{max} (inferred from eddy covariance measurements of surface-atmosphere CO_2 exchange). Hollow circles indicate greenness index; triangles indicate A_{max}. Lines are best-fit interval smoothing splines (smoothing parameter = 11).

improve the reliability of the time series monitoring of vegetation status (Bradley et al., 2010; Ide and Oguma, 2010) and the accuracy of modeling daily GPP.

Digital camera imagery has 3 principal limitations. First, the quality of digital camera images can vary. Sonnentag et al. (2011) have indicated that different commercial digital cameras installed to observe the same ecosystem provide different information. Moreover, Ide and Oguma (2010) have noted a year-to-year drift in color balance and suggested that the color balance varies among cameras produced by different manufacturers. Even if the white balance is fixed in a camera, the inevitable noise due to exposure and weather conditions results in varied greenness indices. Therefore, calibration protocols and standards need to be developed to ensure uniformity in long-term datasets from multiple sites (Ide and Oguma, 2010; Migliavacca et al., 2011).

The second limitation involves the processing of greenness indices. First, different researchers use unique methods to obtain relatively accurate status information about the daily vegetation canopy. For example, Richardson et al. (2009) used mid-day images from 1 camera to calculate the greenness index, Kurc and Benton (2010) used the solar noon images from 3 identical cameras to calculate the average greenness index, and Sonnentag et al. (2011) used the daily mean values from images obtained between 8:00 and 11:00 h local time to calculate the greenness index. In this study, the digital images were obtained every half hour from 8:30 to 17:00 h. The greenness indices are known to change periodically due to seasonal changes in incident light angle and intensity (Fig. 2). Although the minimum-value composite that minimizes the viewing geometries of the canopy between 10:00 and 15:00 h was used in our study to determine the variations in the greenness index data, other approaches need to be explored to determine the best greenness measurement method. Second, outliers produced by unfavorable meteorological conditions must be excluded from the data used to obtain a time series of greenness indices. Different filtering methods can be used to overcome this problem; however, they might introduce new uncertainties. Moreover, in the process of retrieving phenological metrics from the time series of greenness indices, different methods may yield quite different results (White et al., 2009), although we adopted a relatively stable and robust processing method (the double logistic model; Zhu et al., 2012).

The third limitation affecting the modeling of daily GPP is that the parameter values, such as VPD_{min}, VPD_{max}, T_{mmin}, and T_{mmax}, are equal to the values obtained using MODIS data to calculate the daily gross primary productivity mentioned in the User's Guide for GPP and NPP (MOD17A2/A3) Products. In the future, the accuracy of modeled data can be increased by introducing mechanistic experiments.

These limitations should be addressed to improve the time series monitoring of long-term phenological data through the use of digital camera imagery and to identify a feasible method of interpolating high temporal-resolution GPP data. In the future, these advances might facilitate the analysis of the interannual and spatial variability of GPP.

5. Summary

This study showed that high-resolution digital camera images provide reliable information on canopy status. An automated analysis of phenological events was performed by determining the curvature shape of the greenness index to obtain relatively accurate phenological stages. Digital camera imagery expands the scope of phenological observation methods for use in the field and might furnish an effective method of validating remote sensing phenology.

The LUE model developed in this study, which combined information derived from color indices and meteorological data, represents a successful model of daily GPP and might facilitate the monitoring of spatial and temporal variations in carbon uptake.

In conclusion, digital camera imagery can not only provide important information at the site level to improve the understanding of the temporal processes of vegetation canopy dynamics; it can also represent a promising tool for validating different phenological models and hypotheses. However, many limitations still affect image processing, and further efforts are required to address these limitations and establish an optimum method for quantitatively monitoring seasonal crop growth.

Acknowledgments

This study was supported by the National Natural Science Foundation of China (Grant No. 41071251), "Strategic Priority Research Program — Climate Change: Carbon Budget and Relevant Issues" of the Chinese Academy of Sciences (Grant No. XDA05050600), and the Environmental Protection Public Welfare Industry Targeted Research Fund (Grant No. gyh5031103). We thank the anonymous reviewers for their comments and criticisms, which have helped to improve the paper significantly.

References

Adamsen, F.J., Pinter, P.J., Barnes, E.M., LaMorte, R.L., Wall, G.W., Leavitt, S.W., Kimball, B.A., 1999. Measuring wheat senescence with a digital camera. Crop Science 39 (3), 719–724.

Ahrends, H.E., Brugger, R., Stockli, R., Schenk, J., Michna, P., Jeanneret, F., Wanner, H., Eugster, W., 2008. Quantitative phenological observations of a mixed beech forest in northern Switzerland with digital photography. Journal of Geophysical Research — Biogeosciences 113 (G04004), 1–11.

Ahrends, H.E., Etzold, S., Kutsch, W.L., Stoeckli, R., Bruegger, R., Jeanneret, F., Wanner, H., Buchmann, N., Eugster, W., 2009. Tree phenology and carbon dioxide fluxes: use of digital photography at for process-based interpretation the ecosystem scale. Climate Research 39 (3), 261–274.

Arora, V.K., Boer, G.J., 2005. A parameterization of leaf phenology for the terrestrial ecosystem component of climate models. Global Change Biology 11 (1), 39–59.

Baldocchi, D., Falge, E., Gu, L.H., Olson, R., Hollinger, D., Running, S., Anthoni, P., Bernhofer, C., Davis, K., Evans, R., Fuentes, J., Goldstein, A., Katul, G., Law, B., Lee, X.H., Malhi, Y., Meyers, T., Munger, W., Oechel, W., Paw U, K.T., Pilegaard, K., Schmid, H.P., Valentini, R., Verma, S., Vesala, T., Wilson, K., Wofsy, S., 2001. FLUXNET: A new tool to study the temporal and spatial variability of ecosystem-scale carbon dioxide, water vapor, and energy flux densities. Bulletin of the American Meteorological Society 82 (11), 2415–2434.

Booth, D.T., Cox, S.E., Berryman, R.D., 2006. Point sampling digital imagery with "SamplePoint". Environmental Monitoring and Assessment 123 (1–3), 97–108.

Bowers, J.E., Dimmitt, M.A., 1994. Flowering phenology of six woody plants in the northern Sonoran Desert. Bulletin of the Torrey Botanical Society 121 (3), 215–229.

Bradley, E., Roberts, D., Still, C., 2010. Design of an image analysis website for phenological and meteorological monitoring. Environmental Modelling and Software 25 (1), 107–116.

Chandrasekar, K., Sesha Sai, M.V.R., Roy, P.S., Dwevedi, R.S., 2010. Land Surface Water Index (LSWI) response to rainfall and NDVI using the MODIS Vegetation Index product. International Journal of Remote Sensing 31 (15), 3987–4005.

Chen, X., Xu, L., 2012. Temperature controls on the spatial pattern of tree phenology in China's temperate zone. Agricultural and Forest Meteorology 154-155, 195–202.

Chen, X., Hu, B., Yu, R., 2005. Spatial and temporal variation of phenological growing season and climate change impacts in temperate eastern China. Global Change Biology 11 (7), 1118–1130.

Chen, S.Y., Zhang, X.Y., Sun, H.Y., Ren, T.S., Wang, Y.M., 2010. Effects of winter wheat row spacing on evapotranpsiration, grain yield and water use efficiency. Agricultural Water Management 97 (8), 1126–1132.

Chiang, J.-M., Brown, K.J., 2007. Improving the budburst phenology subroutine in the forest carbon model PnET. Ecological Modelling 205 (3), 515–526.

Chmielewski, F.M., Rotzer, T., 2002. Annual and spatial variability of the beginning of growing season in Europe in relation to air temperature changes. Climate Research 19 (3), 257–264.

Crimmins, M.A., Crimmins, T.M., 2008. Monitoring plant phenology using digital repeat photography. Environmental Management 41 (6), 949–958.

Dragoni, D., Schmid, H.P., Wayson, C.A., Potter, H., Grimmond, C.S.B., Randolph, J.C., 2011. Evidence of increased net ecosystem productivity associated with a longer vegetated season in a deciduous forest in south-central Indiana, USA. Global Change Biology 17 (2), 886–897.

Fisher, J., Mustard, J., Vadeboncoeur, M., 2006. Green leaf phenology at Landsat resolution: Scaling from the field to the satellite. Remote Sensing of Environment 100 (2), 265–279.

Frank, M.C., 2003. Phenology and agriculture. In: Schwartz, M.D. (Ed.), Phenology:an Integrative Environmental Science 2003. Kluwer Academic Publishers, MA, pp. 505–522.

Gamon, J.A., Serrano, L., Surfus, J.S., 1997. The photochemical reflectance index: an optical indicator of photosynthetic radiation use efficiency across species, functional types, and nutrient levels. Oecologia 112 (4), 492–501.

Ganguly, S., Friedl, M.A., Tan, B., Zhang, X.Y., Verma, M., 2010. Land surface phenology from MODIS: Characterization of the Collection 5 global land cover dynamics product. Remote Sensing of Environment 114 (8), 1805–1816.

Gitelson, A.A., Peng, Y., Masek, J.G., Rundquist, D.C., Verma, S., Suyker, A., Baker, J.M., Hatfield, J.L., Meyers, T., 2012. Remote estimation of crop gross primary production with Landsat data. Remote Sensing of Environment 121, 404–414.

Graham, E.A., Hamilton, M.P., Mishler, B.D., Rundel, P.W., Hansen, M.H., 2006. Use of a networked digital camera to estimate net CO_2 uptake of a desiccation-tolerant moss. International Journal of Plant Sciences 167 (4), 751–758.

Heinsch, F.A., Reeves, M., Votava, P., Kang, S., Milesi, C., Zhao, M., Glassy, J., Jolly, W.M., Loehman, R., Bowker, C.F., Kimball, J.S., Nemani, R.R., Running, S.W., 2003. User's Guide GPP and NPP (MOD17A2/A3) Products NASA MODIS Land Algorithm.

Heumann, B.W., Seaquist, J.W., Eklundh, L., Jonsson, P., 2007. AVHRR derived phenological change in the Sahel and Soudan, Africa, 1982–2005. Remote Sensing of Environment 108 (4), 385–392.

Hollinger, D.Y., Aber, J., Dail, B., Davidson, E.A., Goltz, S.M., Hughes, H., Leclerc, M.Y., Lee, J.T., Richardson, A.D., Rodrigues, C., Scott, N.A., Achuatavarier, D., Walsh, J., 2004. Spatial and temporal variability in forest–atmosphere CO_2 exchange. Global Change Biology 10 (10), 1689–1706.

Hufkens, K., Friedl, M., Sonnentag, O., Braswell, B.H., Milliman, T., Richardson, A.D., 2012. Linking near-surface and satellite remote sensing measurements of deciduous broadleaf forest phenology. Remote Sensing of Environment 117, 307–321.

Ide, R., Oguma, H., 2010. Use of digital cameras for phenological observations. Ecological Informatics 5 (5), 339–347.

Janssen, P.H.M., Heuberger, P.S.C., 1995. Calibration of process-oriented models. Ecological Modelling 83 (1–2), 55–66.

Jensen, T., Apan, A., Young, F., Zeller, L., 2007. Detecting the attributes of a wheat crop using digital imagery acquired from a low-altitude platform. Computers and Electronics in Agriculture 59 (1–2), 66–77.

Kawashima, S., Nakatani, M., 1998. An algorithm for estimating chlorophyll content in leaves using a video camera. Annals of Botany 81 (1), 49–54.

Kendy, E., Gerard-Marchant, P., Walter, M.T., Zhang, Y.Q., Liu, C.M., Steenhuis, T.S., 2003. A soil–water-balance approach to quantify groundwater recharge from irrigated cropland in the North China Plain. Hydrological Processes 17 (10), 2011–2031.

Kindermann, J., Wurth, G., Kohlmaier, G.H., Badeck, F.W., 1996. Interannual variation of carbon exchange fluxes in terrestrial ecosystems. Global Biogeochemical Cycles 10 (4), 737–755.

Kurc, S.A., Benton, L.M., 2010. Digital image-derived greenness links deep soil moisture to carbon uptake in a creosotebush-dominated shrubland. Journal of Arid Environments 74 (5), 585–594.

Li, J., Yu, Q., Sun, X.M., Tong, X.J., Ren, C.Y., Wang, J., Liu, E.M., Zhu, Z.L., Yu, G.R., 2006. Carbon dioxide exchange and the mechanism of environmental control in a farmland ecosystem in North China Plain. Science in China Series D: Earth Sciences 49, 226–240.

Li, Z.Q., Yu, G.R., Xiao, X.M., Li, Y.N., Zhao, X.Q., Ren, C.Y., Zhang, L.M., Fu, Y.L., 2007. Modeling gross primary production of alpine ecosystems in the Tibetan Plateau using MODIS images and climate data. Remote Sensing of Environment 107 (3), 510–519.

Lieth, H.H., 1976. Contributions to phenology seasonality research. International Journal of Biometeorology 20 (3), 197–199.

Linderholm, H.W., 2006. Growing season changes in the last century. Agricultural and Forest Meteorology 137 (1–2), 1–14.

Liu, J., Pattey, E., 2010. Retrieval of leaf area index from top-of-canopy digital photography over agricultural crops. Agricultural and Forest Meteorology 150 (11), 1485–1490.

Liu, C.M., Yu, J.J., Kendy, E., 2001. Groundwater exploitation and its impact on the environment in the North China Plain. Water International 26 (2), 265–272.

Lukina, E.V., Stone, M.L., Rann, W.R., 1999. Estimating vegetation coverage in wheat using digital images. Journal of Plant Nutrition 22 (2), 341–350.

Menzel, A., Fabian, P., 1999. Growing season extended in Europe. Nature 397 (6721), 659.

Migliavacca, M., Galvagno, M., Cremonese, E., Rossini, M., Meroni, M., 2011. Using digital repeat photography and eddy covariance data to model grassland phenology and photosynthetic CO_2 uptake. Agricultural and Forest Meteorology 151, 1325–1337.

Mirjana, R., Vulić, T., 2005. Important of phenological observations and predictions in agriculture. Journal of Agricultural Sciences 50 (2), 217–225.

Monteith, J.L., 1972. Solar-Radiation and Productivity in Tropical Ecosystems. Journal of Applied Ecology 9 (3), 747–766.

Moulin, S., Kergoat, L., Viovy, N., Dedieu, G., 1997. Global-scale assessment of vegetation phenology using NOAA/AVHRR satellite measurements. Journal of Climate 10 (6), 1154–1170.

Muraoka, H., Koizumi, H., 2005. Photosynthetic and structural characteristics of canopy and shrub trees in a cool-temperate deciduous broadleaved forest: Implication to the ecosystem carbon gain. Agricultural and Forest Meteorology 134 (1–4), 39–59.

Pekin, B., Macfarlane, C., 2009. Measurement of crown cover and leaf area index using digital cover photography and its application to remote sensing. Remote Sensing 1 (4), 1298–1320.

Qin, Z., Yu, Q., Xu, S.H., Hu, B.M., Sun, X.M., Liu, E.M., Wang, J.S., Yu, G.R., Zhu, Z.L., 2005. Water, heat fluxes and water use efficiency measurement and modeling above a farmland in the North China Plain. Science in China Series D: Earth Sciences 48, 207–217.

Richardson, A.D., Jenkins, J.P., Braswell, B.H., Hollinger, D.Y., Ollinger, S.V., Smith, M.L., 2007. Use of digital webcam images to track spring green-up in a deciduous broadleaf forest. Oecologia 152 (2), 323–334.

Richardson, A.D., Braswell, B.H., Hollinger, D.Y., Jenkins, J.P., Ollinger, S.V., 2009. Near-surface remote sensing of spatial and temporal variation in canopy phenology. Ecological Applications 19 (6), 1417–1428.

Richardson, A.D., Anderson, R.S., Arain, M.A., Barr, A.G., Bohrer, G., Chen, G., Chen, J.M., Ciais, P., Davis, K.J., Desai, A.R., Dietze, M.C., Dragoni, D., Garrity, S.R., Gough, C.M., Grant, R., Hollinger, D.Y., Margolis, H.A., McCaughey, H., Migliavacca, M., Monson, R.K., Munger, J.W., Poulter, B., Raczka, B.M., Ricciuto, D.M., Sahoo, A.K., Schaefer, K., Tian, H., Vargas, R., Verbeeck, H., Xiao, J., Xue, Y., 2012. Terrestrial biosphere models need better representation of vegetation phenology: results from the North American Carbon Program Site Synthesis. Global Change Biology 18 (2), 566–584.

Saitoh, T.M., Nagai, S., Saigusa, N., Kobayashi, H., Suzuki, R., Nasahara, K.N., Muraoka, H., 2012. Assessing the use of camera-based indices for characterizing canopy phenology in relation to gross primary production in a deciduous broad-leaved and an evergreen coniferous forest in Japan. Ecological Informatics 11, 45–54.

Sakamoto, T., Shibayama, M., Kimura, A., Takada, E., 2011. Assessment of digital camera-derived vegetation indices in quantitative monitoring of seasonal rice growth. ISPRS Journal of Photogrammetry and Remote Sensing 66 (6), 872–882.

Schwartz, M.D., Reed, B.C., 1999. Surface phenology and satellite sensor-derived onset of greenness: an initial comparison. International Journal of Remote Sensing 20 (17), 3451–3457.

Schwartz, M.D., Reed, B.C., White, M.A., 2002. Assessing satellite-derived start-of-season measures in the conterminous USA. International Journal of Climatology 22 (14), 1793–1805.

Serrano, L., Filella, I., Penuelas, J., 2000. Remote sensing of biomass and yield of winter wheat under different nitrogen supplies. Crop Science 40 (3), 723–731.

Sims, D.A., Rahman, A.F., Cordova, V.D., Baldocchi, D.D., Flanagan, L.B., Goldstein, A.H., Hollinger, D.Y., Misson, L., Monson, R.K., Schmid, H.P., Wofsy, S.C., Xu, L.K., 2005. Midday values of gross CO_2 flux and light use efficiency during satellite overpasses can be used to directly estimate eight-day mean flux. Agricultural and Forest Meteorology 131 (1), 1–12.

Soegaard, H., Jensen, N.O., Boegh, E., Hasager, C.B., Schelde, K., Thomsen, A., 2003. Carbon dioxide exchange over agricultural landscape using eddy correlation and footprint modelling. Agricultural and Forest Meteorology 114 (3–4), 153–173.

Sonnentag, O., Detto, M., Vargas, R., Ryu, Y., Runkle, B.R.K., Kelly, M., Baldocchi, D.D., 2011. Tracking the structural and functional development of a perennial pepperweed (Lepidium latifolium L.) infestation using a multi-year archive of webcam imagery and eddy covariance measurements. Agricultural and Forest Meteorology 151 (7), 916–926.

Soudani, K., Hmimina, G., Delpierre, N., Pontailler, J.Y., Aubinet, M., Bonal, D., Caquet, B., de Grandcourt, A., Burban, B., Flechard, C., Guyon, D., Granier, A., Gross, P., Heinesh, B., Longdoz, B., Loustau, D., Moureaux, C., Ourcival, J.M., Rambal, S., Saint André, L., Dufrêne, E., 2012. Ground-based Network of NDVI measurements for tracking temporal dynamics of canopy structure and vegetation phenology in different biomes. Remote Sensing of Environment 123, 234–245.

Stoner, E.R., Baumgardner, M.F., 1981. Characteristic variations in reflectance of surface soils. Soil Science Society of America Journal 45 (6), 1161–1165.

Studer, S., Stockli, R., Appenzeller, C., Vidale, P.L., 2007. A comparative study of satellite and ground-based phenology. International Journal of Biometeorology 51 (5), 405–414.

Turner, D.P., Ritts, W.D., Cohen, W.B., Gower, S.T., Zhao, M.S., Running, S.W., Wofsy, S.C., Urbanski, S., Dunn, A.L., Munger, J.W., 2003. Scaling Gross Primary Production (GPP) over boreal and deciduous forest landscapes in support of MODIS GPP product validation. Remote Sensing of Environment 88 (3), 256–270.

Veroustraete, F., Sabbe, H., Eerens, H., 2002. Estimation of carbon mass fluxes over Europe using the C-Fix model and Euroflux data. Remote Sensing of Environment 83 (3), 376–399.

White, M.A., Hoffman, F., Hargrove, W.W., Nemani, R.R., 2005. A global framework for monitoring phenological responses to climate change. Geophysical Research Letters 32 (4), 1–4.

White, M.A., de Beurs, K.M., Didan, K., Inouye, D.W., Richardson, A.D., Jensen, O.P., O'Keefe, J., Zhang, G., Nemani, R.R., van Leeuwen, W.J.D., Brown, J.F., de Wit, A., Schaepman, M., Lin, X., Dettinger, M., Bailey, A.S., Kimball, J., Schwartz, M.D., Baldocchi, D.D., Lee, J.T., Lauenroth, W.K., 2009. Intercomparison, interpretation, and assessment of spring phenology in North America estimated from remote sensing for 1982–2006. Global Change Biology 15 (10), 2335–2359.

Wingate, Lisa, Richardson, A.D., Weltzin, Jake F., Nasahara, Kenlo N., Grace, John, 2008. Keeping an eye on the carbon balance: linking canopy development and net ecosystem exchange using a webcam. Fluxletter. 1 (2), 14–17.

Wu, D.R., Yu, Q., Lu, C.H., Hengsdijk, H., 2006. Quantifying production potentials of winter wheat in the North China Plain. European Journal of Agronomy 24 (3), 226–235.

Xiao, X., Hollinger, D., Aber, J., Goltz, M., Davidson, E.A., Zhang, Q., Moore, B., 2004. Satellite-based modeling of gross primary production in an evergreen needleleaf forest. Remote Sensing of Environment 89 (4), 519–534.

Yan, H., Fu, Y., Xiao, X., Huang, H.Q., He, H., Ediger, L., 2009. Modeling gross primary productivity for winter wheat–maize double cropping system using MODIS time series and CO_2 eddy flux tower data. Agriculture, Ecosystems and Environment 129 (4), 391–400.

Zhu, K.Zh., Wan, M.W., 1973. Phenology. Science Press, Beijing.

Zhu, W.Q., Tian, H.Q., Xu, X.F., Pan, Y.Z., Chen, G.S., Lin, W.P., 2012. Extension of the growing season due to delayed autumn over mid and high latitudes in North America during 1982–2006. Global Ecology and Biogeography 21 (2), 260–271.